



HAL
open science

Viscous to Inertial Transition in Dense Granular Suspension

Franco Tapia, Mie Ichihara, Olivier Pouliquen, Élisabeth Guazzelli

► **To cite this version:**

Franco Tapia, Mie Ichihara, Olivier Pouliquen, Élisabeth Guazzelli. Viscous to Inertial Transition in Dense Granular Suspension. *Physical Review Letters*, 2022, 129, 10.1103/physrevlett.129.078001 . hal-03818789

HAL Id: hal-03818789

<https://hal.science/hal-03818789>

Submitted on 18 Oct 2022

HAL is a multi-disciplinary open access archive for the deposit and dissemination of scientific research documents, whether they are published or not. The documents may come from teaching and research institutions in France or abroad, or from public or private research centers.

L'archive ouverte pluridisciplinaire **HAL**, est destinée au dépôt et à la diffusion de documents scientifiques de niveau recherche, publiés ou non, émanant des établissements d'enseignement et de recherche français ou étrangers, des laboratoires publics ou privés.

Viscous to Inertial Transition in Dense Granular Suspension

Franco Tapia^{1,2,3}, Mie Ichihara,¹ Olivier Pouliquen³, and Élisabeth Guazzelli^{3,4}

¹*Earthquake Research Institute, The University of Tokyo, 1-1-1, Yayoi, Bunkyo-ku, Tokyo 113-0032, Japan*

²*Department of Mechanical Systems Engineering, Tokyo University of Agriculture and Technology, Koganei 183-8538, Tokyo, Japan*

³*Aix-Marseille Université, CNRS, IUSTI, 13453 Marseille, France*

⁴*Université Paris Cité, CNRS, Matière et Systèmes Complexes (MSC) UMR 7057, F-75013 Paris, France*

 (Received 23 February 2022; accepted 14 July 2022; published 8 August 2022)

Granular suspensions present a transition from a Newtonian rheology in the Stokes limit to a Bagnoldian rheology when inertia is increased. A custom rheometer that can be run in a pressure- or a volume-imposed mode is used to examine this transition in the dense regime close to jamming. By varying systematically the interstitial fluid, shear rate, and packing fraction in volume-imposed measurements, we show that the transition takes place at a Stokes number of 10 independent of the packing fraction. Using pressure-imposed rheometry, we investigate whether the inertial and viscous regimes can be unified as a function of a single dimensionless number based on stress additivity.

DOI: [10.1103/PhysRevLett.129.078001](https://doi.org/10.1103/PhysRevLett.129.078001)

Dense granular suspensions that consist of concentrated mixtures of noncolloidal particles suspended in a liquid are ubiquitous in many natural phenomena (landslides, debris flows, sediment transport) and industrial processes (concrete, pastes). Their rheology is not fully understood and establishing a unified theoretical framework across the different flowing regimes is still challenging. In the viscous regime [1], the rheology is quasi-Newtonian as the (shear and normal) stresses scale linearly with the shear rate, $\dot{\gamma}$, at a constant volume fraction, ϕ , i.e., exhibiting a viscous scaling $\propto \eta_f \dot{\gamma}$ where η_f is the viscosity of the suspending fluid and with the prefactor being the relative viscosity that is a sole function of ϕ . In the inertial regime for which the exemplary case is a dry granular flow [2], the rheology is Bagnoldian [3] as the stresses scale quadratically with $\dot{\gamma}$, and more precisely vary as $\propto \rho_p d^2 \dot{\gamma}^2$, where ρ_p is the particle density and d their diameter.

The transition between these two regimes where there are a great number of environmental and engineering applications is not well deciphered. It is considered to take place when the viscous and inertial stresses have the same order of magnitude, i.e., to be described by the ratio between the inertial and viscous stress scales, namely the Stokes number $St = \rho_p d^2 \dot{\gamma} / \eta_f$. However, since the seminal work of Bagnold [3], who identified the two regimes, the studies are scarce and still inconclusive. Numerical studies [4–6] find that the transition from viscous (v) to inertial (i) flow happens at a transitional Stokes number $St_{v \rightarrow i} \sim 1-2$ independent of ϕ , while two experiments [7,8] and theoretical work for frictionless particles [9] suggest that $St_{v \rightarrow i}$ vanishes when approaching the jamming transition where $\phi \rightarrow \phi_c$ where ϕ_c is the packing fraction at the jamming transition.

In this Letter, we perform volume-imposed rheometry of dense granular suspensions having suspending fluids of variable viscosity to show unambiguously that the transition from Newtonian to Bagnoldian rheology occurs at $St_{v \rightarrow i} = 10$ independent of ϕ . We then conduct pressure-imposed rheometry [10,11] to examine whether the inertial and viscous regimes can be unified as a function of a single dimensionless number based on stress additivity as suggested by numerical simulations [4,5,12].

The suspensions used in the experiments consisted of large poly(methyl methacrylate) spheres, shown in Fig. 1(a), having mean diameter $d = 4.65$ mm (with a dispersion in size of 1%) and density $\rho_p = 1181$ kg/m³ dispersed in a Newtonian mixture of water, UCON oil, and some amount of sugar insuring density matching with the particles. Four different fluids were used with varying viscosity, $\eta_f = 11, 20, 50,$ and 86 mPa s. Additional negatively buoyant systems involving the sole dry spheres ($\eta_f = 0.0183$ mPa s) and the spheres immersed in pure water ($\eta_f = 1$ mPa s) were used in pressure-imposed rheometry. The properties of these particles were characterized as done in [11]; see the

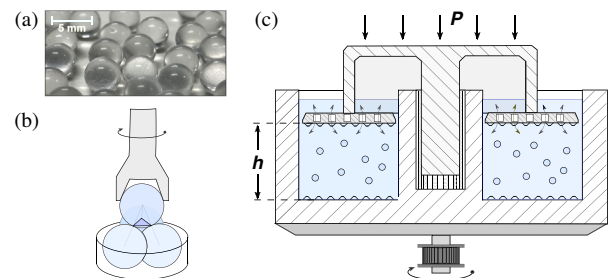


FIG. 1. (a) Image of the poly(methyl methacrylate) spheres. (b) Sketch of the four-ball tribometer. (c) Sketch of the rheometer.

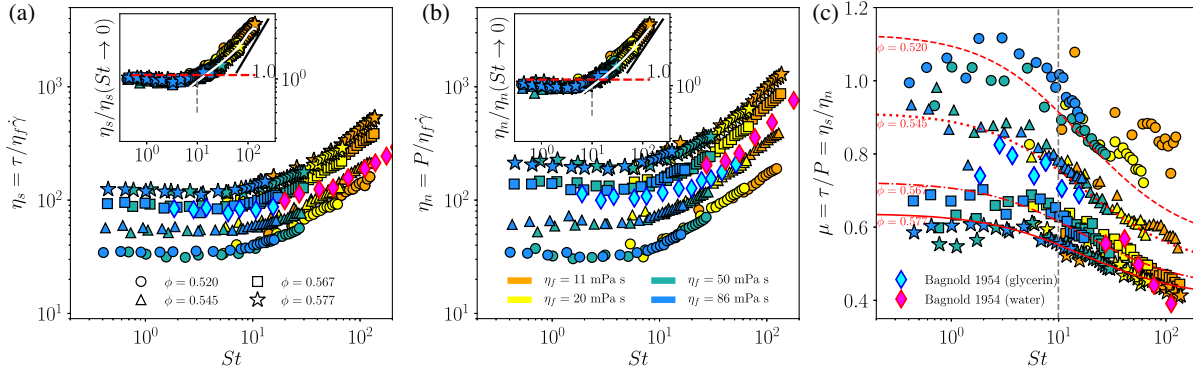


FIG. 2. Rheological data coming from volume-imposed rheometry: (a) $\eta_s = \tau/\eta_f\dot{\gamma}$, (b) $\eta_n = P/\eta_f\dot{\gamma}$, and (c) $\mu = \tau/P = \eta_s/\eta_n$ versus $St = \rho_p d^2 \dot{\gamma} / \eta_f$ for four suspensions having suspending fluids of variable viscosity, $\eta_f = 11$ (orange), 20 (yellow), 50 (green), 86 (blue) mPa s, at four different volume fractions, $\phi = 0.520$ (○), 0.545 (△), 0.567 (□), 0.577 (☆). The data (◇) from Fig. 7 of [3] for spheres having $d = 1.32$ mm and two suspending fluids $\eta_f = 1$ (magenta) and 7 (cyan) mPa s are also reported. Insets of graphs (a),(b): $\eta_s/\eta_n(St \rightarrow 0)$ and $\eta_n/\eta_n(St \rightarrow 0)$ versus St showing a transition from a Newtonian (slope 0) to a Bagnoldian (slope 1) rheology (the white solid lines are the simplest power-law fit of the whole data). Red lines in (c): Constitutive law [Eq. (3)] for the different ϕ with $\phi_c = 0.615$, $\mu_c = 0.31$, $a_\mu = 11.29$, $a_\phi = 0.66$, $\alpha_\mu = 0.0088$, $\alpha_\phi = 0.1$ coming from the pressure-imposed rheology.

Supplemental Material [13] for details. We quantified the particle surface shape with confocal scanning microscopy and found surface roughnesses characterized by an average roughness $R_a = 0.29 \mu\text{m}$ and a standard deviation $R_q = 0.51 \mu\text{m}$. We performed controlled sliding experiments using a four-ball tribological tester monitored by a stress-controlled rheometer (AR2000ex, TA Instruments) [see Fig. 1(b)] and measured a similar interparticle sliding-friction coefficient $\mu_{sf} = 0.47 \pm 0.06$ in dry and water-immersed conditions but a smaller $\mu_{sf} = 0.21 \pm 0.04$ with UCON mixtures.

The rheological measurements were undertaken with a custom rheometer [11] depicted in Fig. 1(c). This shearing device is composed of an annular cylinder (of inner radius 43.95 mm and outer radius 90.28 mm) that is attached to a bottom plate and covered by a top permeable plate. Both plates are made rough by using wire meshes with openings of 6.3 mm corresponding to $1.3d$. The top plate can be moved vertically with a linear positioning stage and enables the fluid to flow through it but not the particles. The bottom plate can be rotated at a constant angular velocity to produce a linear shear. The range of shear rate that can be achieved is $1 \leq \dot{\gamma} \leq 50 \text{ s}^{-1}$. The thickness of the cell, h , can be varied between 24.8 and 27.5 mm, i.e., $5.3d \leq h \leq 6d$. The shear stress, τ , is deduced from measurements of the torque exerted on the top plate after calibration with the pure fluid. The component of the normal stress perpendicular to the top plate, simply referred as the particle pressure P , is given by a precision scale attached to the translation stage after correction for buoyancy. The volume fraction, ϕ , can be deduced from the position of the top plate recorded by a sensor. We estimated the accuracy based on the fluctuations around the stationary values to be 7%, 3%, and ± 0.002 on the measurements of τ , P , and ϕ , respectively. The rheometer could be run in a

pressure-imposed or a volume-imposed mode using a feedback control loop involving the scale measurement or the position of the top plate, respectively. It was operated in an air-conditioned room at 24°C and evaporation of the suspending fluid was inhibited by using a solvent trap covering the cell. The rheological data, data analysis, and plots are given in the Supplemental Material [13].

We start by presenting in Figs. 2(a) and 2(b) the rheological data collected in volume-imposed rheometry for the suspensions having suspending fluids of variable η_f at different ϕ . A Newtonian regime in which the shear and normal viscosities, $\eta_s = \tau/\eta_f\dot{\gamma}$ and $\eta_n = P/\eta_f\dot{\gamma}$, respectively, are independent of St (i.e., independent of $\dot{\gamma}$) but increase with increasing ϕ is observed for $St < 10$. Around $St \approx 10$, the rheology transitions smoothly from Newtonian to continuously shear thickening. For $St > 10$, a Bagnoldian regime in which η_s and η_n scale linearly with St (i.e., with $\dot{\gamma}$) is reached. We have also plotted in Fig. 2(c) the effective friction coefficient $\mu = \tau/P = \eta_s/\eta_n$ versus St . We recover the Stokes regime for $St < 10$. For larger St , μ decreases with increasing St as η_s presents a slower transition to the Bagnoldian regime than η_n .

We have also reported in these graphs the data coming from Fig. 7 of Bagnold's paper [3] obtained in the transition region for a single $\phi = 0.555$ (◇ magenta and cyan). Strikingly, although they were obtained with different particles (spheres of nearly 50% mixture of paraffin wax and lead stearate with $d = 1.32$ mm and ρ_p close to that of water), different fluids (water with $\eta_f = 1$ mPa s and glycerin mixture with $\eta_f = 7$ mPa s), and a different experimental device, these data show a similar transition around $St \approx 10$ and are located in between the present data at $\phi = 0.545$ and 0.567.

The fact the transition takes place at a specific Stokes number independent of ϕ is evidenced in the insets of

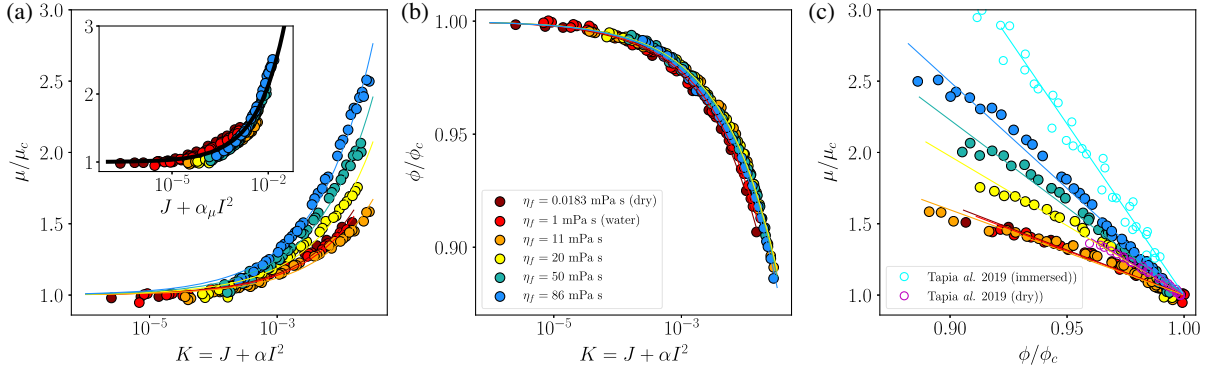


FIG. 3. Rheological data coming from pressure-imposed rheometry: (a) μ/μ_c and (b) ϕ/ϕ_c versus $K = J + \alpha I^2$ with $\alpha = 1/St_{v \rightarrow i}$ and (c) μ/μ_c versus ϕ/ϕ_c for the same neutrally buoyant suspensions as in Fig. 2 and two additional negatively buoyant systems consisting of the sole dry spheres and of the spheres immersed in pure water. The data coming from Fig. 5 of [11] using slightly rough polystyrene sphere (with $d = 580 \mu\text{m}$) in the dry case as well as immersed in a very viscous Newtonian fluid of same density (with $\eta_f = 2.01 \text{ Pa s}$) are also reported. Inset of (a): μ/μ_c versus $J + \alpha_\mu I^2$; the black solid line corresponds to the best fit: $\mu/\mu_c = 1 + a_\mu (J + \alpha_\mu I^2)^{1/2}$ with $a_\mu = 11.29$ and $\alpha_\mu = 0.0088$.

Figs. 2(a) and 2(b) where the viscosities normalized by their values when $St \rightarrow 0$ collapse onto master curves exhibiting the transition from a Newtonian (slope 0) to a Bagnoldian (slope 1) rheology. To find accurately the transitional $St_{v \rightarrow i}$, we choose a threshold value of 3 standard deviations above the mean for the low- St data and compute the point of interception of the horizontal line at this value (horizontal red dashed line) with the simplest power-law fit of the whole data (white solid line). We find $St_{v \rightarrow i} = 10.0$ with an accuracy ± 0.2 and ± 0.5 for $\eta_s(St)$ and $\eta_n(St)$, respectively. An alternative method consisting in finding the interception between a higher-order polynomial fit for the large St and the mean value of the viscosities at low- St regime gives similar transition values; see the Supplemental Material [13].

We now turn to the examination of rheological measurements obtained in pressure-imposed rheometry. When sheared under a confining pressure P , the rheological response of a particulate system is determined by two dimensionless quantities: the effective friction coefficient, $\mu = \tau/P$, and the packing fraction, ϕ . When inertia dominates as for a dry granular flow, these quantities are expected to depend solely upon $I^2 = \rho_p d^2 \dot{\gamma}^2 / P$, which is the ratio of the inertial stress scale $\sim \rho_p d^2 \dot{\gamma}^2$ and the external confinement pressure $\sim P$ [2]. When viscous effects prevail, a viscous stress scale $\sim \eta_f \dot{\gamma}$ should be used instead, and the control parameter is $J = \eta_f \dot{\gamma} / P$ [10]. It has been conjectured [4,5,12] that these two regimes can be unified by using a single dimensionless parameter based on stress additivity, $K = J + \alpha I^2$, and that the transition from viscous to inertial flow happens at a Stokes number $I^2/J = 1/\alpha = St_{v \rightarrow i}$.

In Figs. 3(a) and 3(b), we show the pressure-imposed rheological data for μ and ϕ against $K = J + \alpha I^2$ with $\alpha = 1/St_{v \rightarrow i} = 0.1$ for the same neutrally buoyant suspensions as in Fig. 2 and two additional negatively buoyant systems consisting of the sole dry spheres and of the spheres

immersed in pure water. The data have been normalized by their critical values at jamming, i.e., by the critical friction coefficient, μ_c , and the critical (or maximum flowable) volume fraction, ϕ_c , respectively. These quasi-static values, μ_c and ϕ_c , have been obtained by fitting the data using a linear regression in $K^{1/2}$ (shown by the solid lines) as summarized in Table I; since μ_c and ϕ_c depend on the nature of the frictional contact between the particles, μ_c is smaller and ϕ_c larger in the case of frictional contacts lubricated with UCON mixtures with smaller μ_{sf} . While ϕ/ϕ_c can be expressed as a collapsed function of K given by $\phi/\phi_c = 1 - a_\phi K^{1/2}$ with $a_\phi = 0.66$, there are different curves for μ/μ_c showing a shift in increasing magnitude with increasing η_f . We have attempted to seek a better collapse by having a different value for α . This is obtained by the fit $\mu/\mu_c = 1 + a_\mu (J + \alpha_\mu I^2)^{1/2}$ with $a_\mu = 11.29$ and $\alpha_\mu = 0.0088$, i.e., a larger transitional Stokes number $St_{v \rightarrow i}^\mu \approx 114$, as shown in the inset of Fig. 3(a).

The inability to collapse the data for μ with $\alpha = 1/St_{v \rightarrow i}$ is even more evidenced in Fig. 3(c), where μ/μ_c is plotted against ϕ/ϕ_c and where we have added the data coming from Fig. 5 of [11] using slightly rough polystyrene spheres ($d = 580 \mu\text{m}$ and $\rho_p = 1050 \text{ kg/m}^3$) in the dry case as

TABLE I. Coefficients of the linear regressions in $K^{1/2}$.

η_f (mPa s)	$\mu = \mu_c(1 + a_\mu^K K^{1/2})$		$\phi = \phi_c(1 - a_\phi^K K^{1/2})$	
	μ_c	a_μ^K	ϕ_c	a_ϕ^K
0.0183	0.39	4.76	0.596	0.75
1	0.41	4.41	0.586	0.71
11	0.31	3.79	0.615	0.63
20	0.31	6.07	0.618	0.62
50	0.31	7.85	0.615	0.64
86	0.31	9.96	0.614	0.66

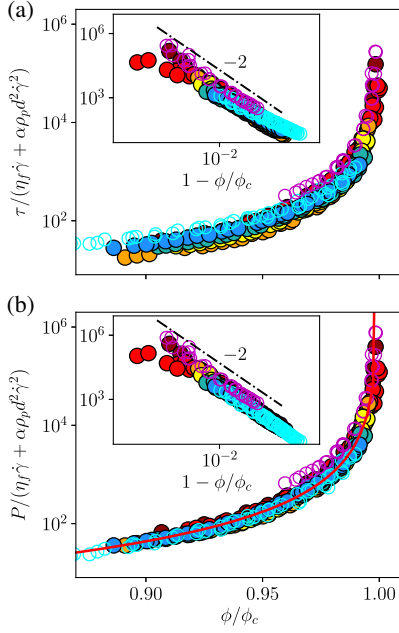


FIG. 4. Rheological data coming from pressure-imposed rheometry: (a) τ and (b) P normalized by $\eta_f \dot{\gamma} + \alpha \rho_p d^2 \dot{\gamma}^2 = \eta_f \dot{\gamma} (1 + \alpha \text{St})$ versus ϕ/ϕ_c (same symbols as in Fig. 3). The insets show these quantities versus the rescaled volume fraction, $1 - \phi/\phi_c$. Red solid line in (b): Constitutive law [Eq. (5)] with $a_\phi = 0.66$.

well as immersed in a very viscous Newtonian fluid of same density ($\eta_f = 2.01$ Pa s). The data align in straight lines jointed at the jamming point, which present an increasing slope with increasing η_f between the two bounds given by the lowest slope for the dry case and the highest slope for the most viscous case.

Although the data of Fig. 3 were obtained under pressure-imposed conditions, τ and P can be inferred and their asymptotic behavior close to the jamming transition examined. Figure 4 shows τ and P normalized by the addition of stress scales, $\eta_f \dot{\gamma} + \alpha \rho_p d^2 \dot{\gamma}^2$, versus ϕ/ϕ_c . These quantities would represent the shear and normal viscosities, $\eta_s(\phi) = \tau/\eta_f \dot{\gamma}$ and $\eta_n(\phi) = P/\eta_f \dot{\gamma}$, in the purely viscous Newtonian regime and ϕ -dependent functions, $\eta_I(\phi) = \tau/\rho_p d^2 \dot{\gamma}^2$ and $\eta_{II}(\phi) = P/\rho_p d^2 \dot{\gamma}^2$, in the purely Bagnoldian regime [11]. The collapse is excellent for P but poorer for τ . This is due to the imperfect collapse of μ , seen in Fig. 3(c), since $\tau = \mu P$. Note that this gives only small shifts between the different curves in the τ graph as the values of μ are orders of magnitude smaller than those of τ and P . The important output shown in the insets is that the normalized τ and P functions diverge as $(1 - \phi/\phi_c)^{-2}$. The fact that a same divergence is observed across the viscous and inertial regimes shows that the crossover shear rate, $\dot{\gamma}_{v \rightarrow i} \sim (\eta_f/\rho_p d^2) \eta_s(\phi)/\eta_I(\phi)$, or similarly $\sim (\eta_f/\rho_p d^2) \eta_n(\phi)/\eta_{II}(\phi)$, is independent of ϕ close to the jamming transition. This confirms the finding

of a crossover Stokes number independent of ϕ obtained in volume-imposed rheometry in Figs. 2(a) and 2(b).

In this work, we have explored the viscous to inertial transition in dense granular suspensions. The first major output coming from volume-imposed rheology is the finding of a crossover from viscous to inertial flow at a Stokes number independent of the packing fraction, $\text{St}_{v \rightarrow i} = 10$. This is consistent with the data of Bagnold for suspensions having similar large spheres [3] but strongly differs from the experimental results of [7,8], which report decade smaller $\text{St}_{v \rightarrow i} \sim 10^{-3} - 10^{-2}$ for suspensions consisting of much smaller spheres that are potentially nonfrictional and prone to colloidal interactions. In this latter case of frictionless spheres, theoretical calculations [9] can be undertaken and suggests that the divergence of $\eta_s(\phi)$ is slower than that of $\eta_I(\phi)$, and thus that $\dot{\gamma}_{v \rightarrow i} \rightarrow 0$ as $\phi \rightarrow \phi_c$, i.e., the transition occurs at a very small Stokes number when approaching jamming. In the present case of frictional spheres, the similar divergence of the functions $\eta_s(\phi)$ and $\eta_I(\phi)$ leads to $\dot{\gamma}_{v \rightarrow i}$ and consequently $\text{St}_{v \rightarrow i}$ independent of ϕ , as noted above in the discussion of Fig. 4. This qualitatively agrees with numerical simulations of frictional spheres [4–6], which, however, find a slightly smaller $\text{St}_{v \rightarrow i} \sim 1-2$. Theoretical studies are yet unable to fully assess the role played by friction. The second important result coming from pressure-imposed rheology has been to find that the packing fraction is governed by the single dimensionless number $J + \alpha_\phi I^2$ with $\alpha_\phi = \alpha = 1/\text{St}_{v \rightarrow i} = 0.1$ but not the effective friction, which seems to be governed instead by $J + \alpha_\mu I^2$ with a smaller $\alpha_\mu = 0.0088$ characteristic of a larger $\text{St}_{v \rightarrow i}^\mu \approx 114$. The existence of two distinct scalings for ϕ and μ is not captured by the numerical simulations for frictional particles [4–6], which may not encompass the full hydrodynamics across the flow regimes.

We can then attempt to rationalize the data by proposing the constitutive laws in the dense regime close to jamming,

$$\mu = \mu_c [1 + a_\mu (J + \alpha_\mu I^2)^{1/2}], \quad (1)$$

$$\phi = \phi_c [1 - a_\phi (J + \alpha_\phi I^2)^{1/2}], \quad (2)$$

for the pressure-imposed rheology. These relations lead to

$$\mu = \mu_c \left[1 + \frac{a_\mu}{a_\phi} \left(1 - \frac{\phi}{\phi_c} \right) \sqrt{(1 + \alpha_\mu \text{St}) / (1 + \alpha_\phi \text{St})} \right], \quad (3)$$

which agrees well with the volume-imposed data of Fig. 2(c), even though the range of ϕ is lower than that of the pressure-imposed data. The shear and normal stresses are then

$$\tau = \mu(\phi, \text{St}) P(\phi, \text{St}), \quad (4)$$

$$P = \eta_f \dot{\gamma} (1 + \alpha_\phi \text{St}) a_\phi^2 (1 - \phi/\phi_c)^{-2}, \quad (5)$$

in agreement with the scaling and asymptotic behavior seen in Fig. 4. The slower transition of τ compared to that of P is embedded in $\mu(\phi, \text{St})$, which describes the anisotropy of the stresses and may reflect changes in the suspension microstructure and in the nature of the particle interactions when increasing inertia. The proposed empirical rheology is derived for steady and uniformly sheared flows but can be further used as a basis for developing more complex rheology encompassing nonlocal effects [14].

We greatly thank M. Kameda and O. Kuwano for discussions and W. Lecoz and S. Noël for technical assistance. This work was supported by the JSPS KAKENHI Grant No. 19H00713. F.T. is supported by the visiting researcher program of the Earthquake Research Institute.

-
- [1] É. Guazzelli and O. Pouliquen, Rheology of dense granular suspensions, *J. Fluid Mech.* **852**, P1 (2018).
 - [2] Y. Forterre and O. Pouliquen, Flows of dense granular media, *Annu. Rev. Fluid Mech.* **40**, 1 (2008).
 - [3] R. A. Bagnold, Experiments on a gravity-free dispersion of large solid spheres in a Newtonian fluid under shear, *Proc. R. Soc. A* **225**, 49 (1954).
 - [4] M. Trulsson, B. Andreotti, and P. Claudin, Transition from the Viscous to Inertial Regime in Dense Suspensions, *Phys. Rev. Lett.* **109**, 118305 (2012).

- [5] L. Amarsid, J.-Y. Delenne, P. Mutabaruka, Y. Monerie, F. Perales, and F. Radjaï, Viscoinertial regime of immersed granular flows, *Phys. Rev. E* **96**, 012901 (2017).
- [6] C. Ness and J. Sun, Flow regime transitions in dense non-Brownian suspensions: Rheology, microstructural characterization, and constitutive modeling, *Phys. Rev. E* **91**, 012201 (2015).
- [7] A. Fall, A. Lemaître, F. Bertrand, D. Bonn, and G. Ovarlez, Shear Thickening and Migration in Granular Suspensions, *Phys. Rev. Lett.* **105**, 268303 (2010).
- [8] Y. Madraki, A. Oakley, A. Nguyen Le, A. Colin, G. Ovarlez, and S. Hormozi, Shear thickening in dense non-brownian suspensions: Viscous to inertial transition, *J. Rheol.* **64**, 227 (2020).
- [9] E. DeGiuli, G. Düring, E. Lerner, and M. Wyart, Unified theory of inertial granular flows and non-Brownian suspensions, *Phys. Rev. E* **91**, 062206 (2015).
- [10] F. Boyer, É. Guazzelli, and O. Pouliquen, Unifying Suspension and Granular Rheology, *Phys. Rev. Lett.* **107**, 188301 (2011).
- [11] F. Tapia, O. Pouliquen, and É. Guazzelli, Influence of surface roughness on the rheology of immersed and dry frictional spheres, *Phys. Rev. Fluids* **4**, 104302 (2019).
- [12] T. T. Vo, S. Nezamabadi, P. Mutabaruka, J.-Y. Delenne, and F. Radjaï, Additive rheology of complex granular flows, *Nat. Commun.* **11**, 1476 (2020).
- [13] See Supplemental Material at <http://link.aps.org/supplemental/10.1103/PhysRevLett.129.078001> for the characterization of the particle properties as well as the rheological data and data analysis.
- [14] K. Kamrin, Non-locality in granular flow: Phenomenology and modeling approaches, *Front. Phys.* **7**, 116 (2019).